

Kink-Antikink Interaction Forces and Bound States in a Biharmonic ϕ^4 Model

Robert J. Decker,¹ A. Demirkaya,¹ N. S. Manton,² and P. G. Kevrekidis^{3,4}

¹*Mathematics Department, University of Hartford,
200 Bloomfield Ave., West Hartford, CT 06117, USA*

²*Department of Applied Mathematics and Theoretical Physics,
University of Cambridge, Wilberforce Road, Cambridge CB3 0WA, U.K.*

³*Department of Mathematics and Statistics, University of Massachusetts, Amherst, MA 01003-4515, USA*

⁴*Mathematical Institute, University of Oxford, Oxford, UK*

We consider the interaction of solitons in a biharmonic, beam model analogue of the well-studied ϕ^4 Klein-Gordon theory. Specifically, we calculate the force between a well separated kink and antikink. Knowing their accelerations as a function of separation, we can determine their motion using a simple ODE. There is good agreement between this asymptotic analysis and numerical computation. Importantly, we find the force has an exponentially-decaying oscillatory behaviour (unlike the monotonically attractive interaction in the Klein-Gordon case). Corresponding to the zeros of the force, we predict the existence of an infinite set of field theory equilibria, i.e., kink-antikink bound states. We confirm the first few of these at the PDE level, and verify their anticipated stability or instability. We also explore the implications of this interaction force in the collision between a kink and an oppositely moving antikink.

I. INTRODUCTION

The symmetry-breaking ϕ^4 potential has a time-honoured history in the context of nonlinear partial differential equations (PDE), especially of the Klein-Gordon type [1, 2]. In nonlinear Klein-Gordon theory, the interaction and collisions of kinks and antikinks remains a somewhat elusive topic [3], and research into this is (still) ongoing [4, 5]. This theory combines a Laplacian with a ϕ^4 potential, and it is well-known that kinks and antikinks attract [6]. Yet the interplay of translational, internal and extended (phonon) modes at relatively high speeds [7–12], leading to fractal, so-called multi-bounce collision windows, still eludes a self-consistent, low-dimensional effective particle description. The reader is referred to [13] for a summary of recent developments on the subject.

The standard ϕ^4 Klein-Gordon theory yields the field equation

$$u_{tt} = u_{xx} - V'(u), \quad (1)$$

where $V(u) = \frac{1}{2}(u^2 - 1)^2$. In this paper, we further explore a variant, referred to as the nonlinear beam model [14, 15]. Here, the harmonic spatial derivative term is replaced by a biharmonic term, and the field equation is

$$u_{tt} = -u_{xxxx} - V'(u), \quad (2)$$

with $V(u)$ as before.

Similar variant models have been recently considered by a number of authors [16–19]. They have potential applications to the propagation of travelling waves in suspension bridges; there, the models often involve piecewise constant or exponential nonlinearities. Part of our interest stems from a recent development in the realm of nonlinear Schrödinger (NLS) equations, of which the real-field equation considered here is a simplification. In particular, in the context of nonlinear optics, the possibility of the so-called pure quartic solitons has *experimentally* showcased the potential of quartic dispersion combined with cubic nonlinearities, similar to what we study here [20]. Moreover, a very recent extension has considered combining harmonic and biharmonic terms [21], and it is interesting to note that linearized models of this mixed type occur in the context of stiff strings and piano tuning [22]. Finally, the existence and stability of standing waves in certain NLS models [23] may be connected with the real field phenomena found here.

In earlier work [14, 15], some of the present authors explored the existence, asymptotic tail properties, and stability of both static and travelling single kinks, and complemented this with a numerical investigation of kink-antikink collisions as a function of the incoming speeds. We found no multi-bounce windows or accompanying fractal structure. We did, however, find an intriguing oscillatory behaviour in the velocity-out (i.e., outgoing velocity) versus velocity-in (incoming velocity) graph at the boundaries of the bound state interval of velocity-in values.

Here, we extend our study of the dynamics of kinks and antikinks in this beam model – a biharmonic nonlinear field theory. Specifically, we first calculate the asymptotic force and associated interaction potential between a kink and antikink, using the method of [6]. Using our knowledge that the single kink (and antikink) tails are spatially oscillatory and exponentially decaying [15], we derive an explicit formula for the force. In contrast to the harmonic case, we find that as a function of separation the sign of the force alternates between a sequence of zeros. The force is *not* universally attractive as in harmonic field theories, but rather alternates between attractive and repulsive. The consequence is the existence of a sequence of equilibria, i.e., bound states of a kink and antikink. A topological constraint forces these equilibria to alternate between local maxima and minima in the potential energy landscape, i.e., between saddles and centers of the associated dynamical system. There is a self-similar pattern of progressively (exponentially) smaller basins between adjacent saddles where the kink and antikink can be trapped in an oscillatory motion. We then confirm these predictions by full eigenvalue computations around the equilibria, and also by solving the dynamical PDE for the field. The features we have discovered are novel, to the best of our knowledge, and it is interesting to explore if they persist in settings involving mixed harmonic and biharmonic terms (and, of course, beyond Klein-Gordon models).

In Sec. II, we present the basic mathematical features of the beam model – the Lagrangian and Hamiltonian, and the conservation laws of energy and momentum – and explain how to adapt the ideas of [6] to the present biharmonic setting. We then derive a formula for the acceleration of a well-separated kink and antikink, as a function of their separation. In Sec. III, we present results of a systematic numerical investigation of the kink-antikink solutions of the field theory PDE, and compare the asymptotic, analytical predictions. We also examine the implications for kink-antikink collisions. Finally, in Sec. IV, we summarize our findings and outline some future challenges.

II. THEORY OF THE KINK-ANTI-KINK INTERACTION

For our nonlinear beam model, the Lagrangian density is

$$\mathcal{L}(u; t) = \mathcal{T}(u; t) - \mathcal{V}(u; t) = \frac{1}{2}u_t^2 - \left(\frac{1}{2}u_{xx}^2 + V(u) \right), \quad (3)$$

and the Lagrangian is

$$L = \int_{-\infty}^{\infty} \mathcal{L} dx = \int_{-\infty}^{\infty} \left(\frac{1}{2}u_t^2 - \frac{1}{2}u_{xx}^2 - V(u) \right) dx, \quad (4)$$

leading to the field equation Eq. (2). Naturally, the corresponding Hamiltonian is

$$\mathcal{H}(u; t) = \int_{-\infty}^{\infty} (\mathcal{T}(u; t) + \mathcal{V}(u; t)) dx = \int_{-\infty}^{\infty} \left(\frac{1}{2}u_t^2 + \frac{1}{2}u_{xx}^2 + V(u) \right) dx. \quad (5)$$

The momentum on the interval $[x_1, x_2]$ is given by the standard expression

$$P = - \int_{x_1}^{x_2} u_t u_x dx. \quad (6)$$

When x_1 and x_2 tend to $-\infty$ and ∞ , P is the total momentum, and using the field equation, one can show that this is conserved. Here, we will instead use Eq. (6) in a more limited spatial range, in the spirit of the calculation of [6], in order to calculate the force that a kink exerts on an antikink.

Differentiating P with respect to time t , and using Eq. (2), we find that

$$\begin{aligned} \frac{dP}{dt} &= - \int_{x_1}^{x_2} (u_{tt}u_x + u_t u_{xt}) dx \\ &= \int_{x_1}^{x_2} \left(u_{xxxx}u_x + V'(u)u_x - \frac{1}{2}(u_t^2)_x \right) dx \\ &= \left[u_x u_{xxx} - \frac{1}{2}u_{xx}^2 + V(u) - \frac{1}{2}u_t^2 \right]_{x_1}^{x_2}, \end{aligned} \quad (7)$$

where the quantity in square brackets is the component T_{xx} of the energy-momentum tensor [24]. The last expression can be interpreted as the force F acting on the part of the field between x_1 and x_2 . For a field configuration $u(x, t) = \varphi(x)$ that is static or almost so, we can ignore the term involving u_t^2 , and the force becomes

$$F = \left[\varphi_x \varphi_{xxx} - \frac{1}{2}\varphi_{xx}^2 + V(\varphi) \right]_{x_1}^{x_2}. \quad (8)$$

The quantity in square brackets is now the first integral of the static field equation $\varphi_{xxxx} + V'(\varphi) = 0$, so it is a constant, independent of x , if $\varphi(x)$ satisfies this equation. Therefore there is no force acting on any part of an exact static solution, consistent with the momentum P of such a state being zero and remaining so. However, we are interested in the non-zero force for a kink-antikink configuration $\varphi(x)$ that is only static instantaneously.

So, consider a concrete field configuration $\varphi(x)$ that is a superposition of a kink solution centered at $-X$ and an antikink centered at X , where X is large and positive so the antikink-kink separation $2X$ is large. The fields of the individual kink and antikink are $\varphi_K(x+X)$ and $\varphi_{AK}(x-X) = -\varphi_K(x-X)$, where $\varphi_K(x)$ denotes the kink centered at the origin. Their superposition is

$$\varphi(x) = \varphi_K(x+X) + \varphi_{AK}(x-X) - 1. \quad (9)$$

The shift by -1 is required to satisfy the boundary conditions $\varphi(x) \rightarrow -1$ as $x \rightarrow \pm\infty$.

In the region between the kink and antikink, near $x = 0$, $\varphi(x)$ is a superposition of the kink and antikink tail fields. Let us write $\varphi_K(x) = 1 - \eta_K(x)$. For large positive x , the kink tail $\eta_K(x)$ is spatially oscillatory and exponentially small. Its precise form is $\eta_K(x) = be^{-x} \cos(x-d)$, where the parameters have been determined numerically in [15] to be $b \approx 0.9650$ and $d \approx 0.4086$. Then, in the region between the kink and antikink we can write $\varphi(x) = 1 - \eta(x)$ where

$$\eta(x) = \eta_K(x+X) + \eta_{AK}(x-X). \quad (10)$$

η_{AK} , the tail of the antikink (to its left) is the reflection of η_K , the tail of the kink (to its right).

To find the force on the antikink, due to the kink, we need to evaluate for the field configuration $\varphi(x)$ the expression F above, setting $x_1 = 0$ and $x_2 \rightarrow \infty$. The contribution from x_2 vanishes, as the field derivatives all vanish there, and so does V because φ satisfies the boundary conditions. At $x_1 = 0$, φ differs from 1 by the sum of the exponentially small tails, so we can replace $V(\varphi)$ by $V(1 - \eta) \simeq 2\eta^2$. The derivatives of φ are minus the derivatives of η , so the force simplifies to the quadratic expression

$$F = -\eta_x \eta_{xxx} + \frac{1}{2} \eta_{xx}^2 - 2\eta^2. \quad (11)$$

The right hand side of F is now the first integral of the linearized static field equation, $\eta_{xxxx} + 4\eta = 0$. The kink tail η_K satisfies this equation, and also decays exponentially as x increases, so for η_K by itself the force is zero; similarly so for the antikink tail η_{AK} , which decays exponentially as x decreases. These self-forces can also be shown to be zero by direct calculation. For $\eta = \eta_K + \eta_{AK}$, it is therefore only the cross terms (the interaction terms) that give a non-zero force, so

$$F = -(\eta_K)_x (\eta_{AK})_{xxx} - (\eta_K)_{xxx} (\eta_{AK})_x + (\eta_K)_{xx} (\eta_{AK})_{xx} - 4(\eta_K)(\eta_{AK}). \quad (12)$$

Note that since $\eta(x)$, the sum of the tails, also satisfies the linearized static field equation, this force is independent of where it is evaluated in the region between the kink and antikink. For convenience, we are evaluating it at $x = 0$.

The tail of the kink centered at $-X$ is $\eta_K(x + X) = be^{-(x+X)} \cos(x + X - d)$, and its derivatives are

$$\begin{aligned} (\eta_K)_x &= -be^{-(x+X)} (\cos(x + X - d) + \sin(x + X - d)) \\ (\eta_K)_{xx} &= 2be^{-(x+X)} \sin(x + X - d) \\ (\eta_K)_{xxx} &= 2be^{-(x+X)} (\cos(x + X - d) - \sin(x + X - d)). \end{aligned} \quad (13)$$

The tail of the antikink centred at X is $\eta_{AK}(x - X) = be^{x-X} \cos(x - X + d)$, and its derivatives are similar. Combining the results for η_K and η_{AK} , and using a trigonometric addition formula, we find, finally, that the force that the kink exerts on the antikink is

$$F = -8b^2 e^{-2X} \cos(2X - 2d). \quad (14)$$

The kink at $-X$ experiences the opposite force.

The inertial mass of a single kink or antikink can be found from its momentum P . Suppose a kink is centered at the moving point $X(t)$ and that \dot{X} is small, so the kink profile is approximately that of a static kink. Then $u(x, t) = \varphi_K(x + X(t))$, and from Eq. (6) we see that the kink momentum is $M\dot{X}$, where

$$M = \int_{-\infty}^{\infty} (\varphi_K)_x^2 dx. \quad (15)$$

A similar calculation of the kinetic energy of a moving kink gives $\mathcal{T} = \frac{1}{2} M \dot{X}^2$. Numerically, it has been determined that $M \approx 1.1852$. Note that M is not the static energy of the kink; this is consistent in a theory without Lorentz invariance (contrary, e.g., with the situation in the nonlinear Klein-Gordon models such as Eq. (1)).

The equation of motion for the antikink is therefore

$$M\ddot{X} = -8b^2 e^{-2X} \cos(2X - 2d). \quad (16)$$

The separation $s = 2X$ obeys the equation $\frac{1}{2} M \ddot{s} = -8b^2 e^{-s} \cos(s - 2d)$; as usual for two bodies of equal mass M , this involves the reduced mass $\frac{1}{2} M$. Using the parameter values M, b and d given above, we find the acceleration of the antikink is

$$\ddot{X} = -6.286e^{-2X} \cos(2X - 0.8172). \quad (17)$$

This asymptotic analytical result will be compared with the result of a direct numerical computation in the next section.

III. NUMERICAL RESULTS

As in [15] we use Fourier-based spectral methods [25] to discretize Eq. (2) in the spatial direction. Here we use the interval $x \in [-50, 50]$ with an increment of $\Delta x = 0.2$. We couple this with Matlab's built-in ODE solver *ode45* to create our PDE simulations, and again *ode45* for the ODE simulations.

A. Kink-Antikink Acceleration and Equilibrium Solutions

In this section, we employ the method developed in [26] to determine the force (as measured by the acceleration) between an initially stationary kink and antikink as a function of x_0 (half of the separation distance). Similar to [26], we find $\varphi_{\min}(x_0)$ which minimizes the quantity $\|\varphi^{(4)} + V'(\varphi)\|_2^2$ subject to keeping the positions of the kink and antikink (and hence x_0) constant, using nonlinear least squares (*lsqnonlin* in Matlab).

For the initial trial input in *lsqnonlin* we make use of static solutions to Eq. (1). In particular, if $u_0(x)$ is a static kink in the ϕ^4 Klein-Gordon model (given by $u_0(x) = \tanh(x)$) then we use

$$u(x) = u_0(x + x_0) + U(x)(-u_0(x - x_0) - u_0(x + x_0)) \quad (18)$$

as the initializer (called the split-domain ansatz in [26]), where $U(x)$ is the Heaviside function. This ansatz, which represents a ϕ^4 kink and antikink separated by a distance of $2x_0$, is sufficiently similar to the corresponding configuration of a beam kink and antikink to converge to the desired result.

Then we use $\varphi_{\min}(x_0)$ as the initial condition (along with zero initial velocity) in Eq. (2), and allow this initial configuration to evolve for a short period of time (0.01 time units). We track the center of the kink $X_K(x_0, t)$ (left-side intersection of the PDE solution curve $u(x, t)$ with $u = 0$) and find that during this time interval the velocity $V_K(x_0, t)$ of the kink depends nearly linearly on time (we use $X_{AK}(x_0, t)$ and $V_{AK}(x_0, t)$ for the position and velocity of the antikink). We then use the slope of the velocity versus time graph to measure the initial acceleration of the kink $A_K(x_0)$ (similarly, $A_{AK}(x_0)$ represents the initial acceleration of the antikink).

In Figure 1, upper left panel, we show the acceleration of the kink $A_K(x_0)$ as a function of x_0 for values of x_0 in the range $[0.2, 9.0]$; in an inset of that figure we show the same data set, but this time for x_0 in the range $[1.8, 9.0]$. Examination of the raw data shows that oscillations continue and that the acceleration changes sign in regular intervals (for example, the inset shows that the data becomes positive again in the interval $[2, 4]$). Thus the data appears to have the shape of damped harmonic motion. Assuming that the acceleration data may fit a model of the form $A_K(x_0) = ae^{-bx_0} \cos(cx_0 + d)$, we find five data values $(x_0, A_K(x_0))$ that represent local maxima or minima of the acceleration, and fit a linear equation to $(x_0, \ln(\text{abs}(A_K(x_0))))$ in order to approximate b . The result is shown in the upper right panel of Figure 1. The fit is good with a slope of approximately $b = -2$, and so we multiply the raw data by e^{2x_0} , expecting a shifted cosine curve to emerge; we see that this is the case in the plot in the bottom left panel of Figure 1. This plot indicates that the model is working well for x_0 values greater than about $x = 1.8$, and so we fit a shifted cosine curve to that part of the data and lay the fitted curve on top of the data for an excellent fit. For $x_0 < 1.8$, the kink and antikink begin to merge and the concept of an acceleration or a force between them loses meaning.

In the bottom right panel of Figure 1 we show the model

$$A_K(x_0) = 6.389e^{-2x_0} \cos(2x_0 - 0.81590) \quad (19)$$

that results from the original acceleration data (with the same data as the inset for the top left panel). The values of x_0 where the acceleration is zero should correspond to static equilibria of Eq. (2). In between the equilibrium solutions, the kink and antikink should either approach each other ($A_K(x_0)$ positive, $A_{AK}(x_0)$ negative) or drift apart ($A_K(x_0)$ negative, $A_{AK}(x_0)$ positive). This should result in regions of x_0 values, where steady oscillations occur around centers, lying between adjacent saddles in the potential energy landscape.

In detail, we expect that the motion of the center $X_{AK}(x_0, t)$ of the antikink will obey the simple ODE (as long as $X_{AK}(x_0, t) \geq 1.8$)

$$\ddot{X}_{AK} + 6.389e^{-2X_{AK}} \cos(2X_{AK} - 0.8159) = 0. \quad (20)$$

This is because the antikink has acceleration opposite that of the kink and the position of the antikink ($X_{AK}(x_0, t)$) is equal to half of the separation between the kink and antikink (i.e. $X_{AK}(x_0, 0) = x_0$). Notice the remarkable agreement of this result with the asymptotic prediction of Eq. (17). We now further explore the validity and implications of this for the nonlinear PDE, Eq. (2).

Using the results summarized in Figure 1 we should find static solutions of Eq. (2) near the zeros of $\cos(2x - 0.8159)$. The first six such zeros are at $x = 1.19, 2.76, 4.33, 5.91, 7.48, 9.04$. We can use Matlab's *fsolve* command on the system $D_2^2 u + V'(u) = 0$ with an initializer that is close to the desired equilibrium solution in order for *fsolve* to converge to that solution. For the initializer we use Eq. (18) again, with x_0 close to one of the above zeros. Note that the value of x_0 moves significantly from $x_0 = 1.19$ in the initializer to $x_0 = 1.30$ in the *fsolve* full solution for the first case (because we are in the region $x < 1.8$ where the asymptotic fit is breaking down); for the other cases, there is negligible change. See Figure 2 for the first four equilibrium solutions. Note that there is no further solution with x_0 smaller.

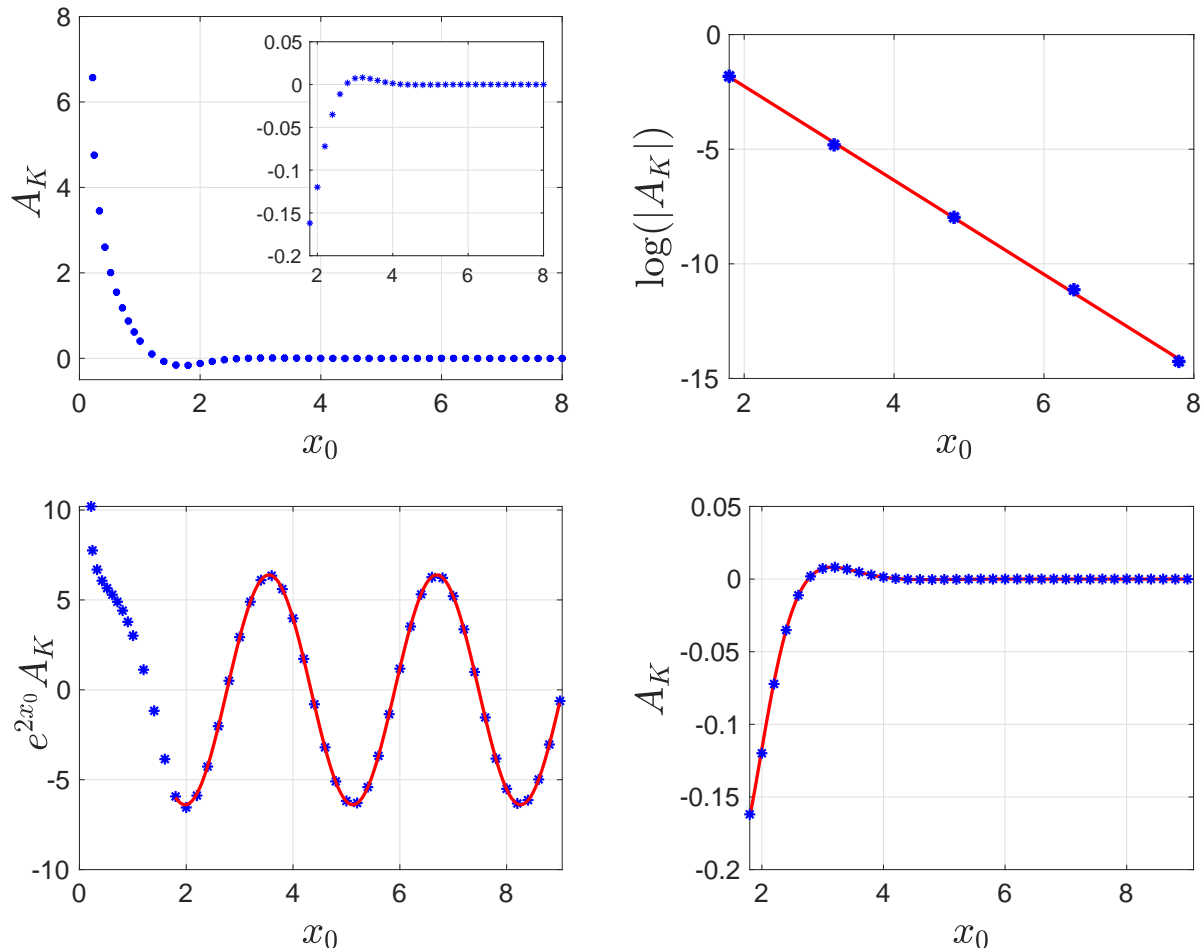


FIG. 1. Top left panel shows the acceleration of the kink A_K vs half-separation x_0 . Top right panel shows the x_0 values of local maxima/minima of acceleration data vs the log of absolute value of the acceleration data (blue stars) and the fitted line $y = -2.051x_0 + 1.848$ (red solid line). Bottom left panel shows $e^{2x_0} A_K$ vs x_0 on the interval $[1.8, 9]$ (blue stars) and the fitted curve $y = 6.389 \cos(2x - 0.81590)$ (red solid curve). Bottom right panel shows A_K vs x_0 on the interval $[1.8, 9]$ (blue stars) and the fitted curve $y = 6.389e^{-2x_0} \cos(2x_0 - 0.81590)$ (red solid curve).

Furthermore, we should be able to predict the local stability of each of the equilibrium solutions using Equation (20). When x_0 is in one of the intervals $(0, 1.30)$, $(2.76, 4.33)$, $(5.91, 7.48)$ the acceleration $A_{AK}(x_0)$ of the antikink is negative (since the kink acceleration is positive there), and when x_0 is in one of the intervals $(1.30, 2.76)$, $(4.33, 5.91)$, $(7.48, 9.04)$, $A_{AK}(x_0)$ is positive. Thus a kink starting at rest in the interval $(0, 1.30)$ or $(1.30, 2.76)$ will tend to start moving away from $x = 1.30$ indicating a saddle point in the phase portrait of Equation (20). A kink starting at rest in $(1.30, 2.76)$ or $(2.76, 4.33)$ will tend to move towards $x = 2.76$ indicating a center at that point. Similarly we expect saddles at $x = 4.33$ and 7.48 and centers at $x = 5.91$ and $x = 9.04$.

For another perspective on the equilibrium solutions shown in Figure 2, their stability, and their relationship to the acceleration curve in Figure 1, we proceed as follows. Multiplying the acceleration term in Eq. (20) by $2M$ ($M = 1.18519$, calculated numerically) and then integrating it gives the potential energy graph. We can then calculate the field-theoretic potential energy of each of the equilibrium solutions as $\int_{-\infty}^{\infty} (\frac{1}{2}u_{xx}^2 + V(u))dx$ (after which we normalize by subtracting the limiting value at infinite separation, about 2.099666, to make the limiting value of the interaction potential zero). We then plot these points along with the potential energy graph in Figure 3. We see that the potential energy of the equilibria occurs at the maximum or minimum points on the potential energy graph. The leftmost point, while still lying on the graph, is not quite at the nearby maximum. This is not unexpected, as it was shown in Figure 1 that a good fit to the asymptotic data does not begin until about $x_0 = 2$. The maxima are the unstable equilibria (saddles), and the minima are the stable equilibria (centers), as expected.

Figure 4 shows the phase portrait of Eq. (20) for different intervals on the $X_{AK}(x_0)$ axis and different scales along

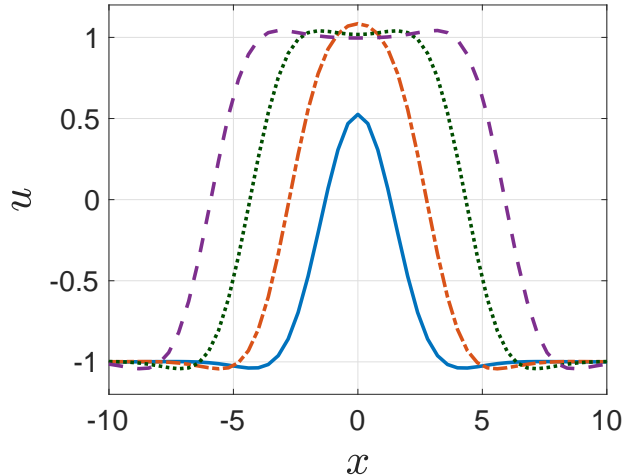


FIG. 2. Static, equilibrium solutions corresponding to $x_0 = 1.30$ (blue solid curve), $x_0 = 2.76$ (orange dash-dot curve), $x_0 = 4.34$ (green dot curve), $x_0 = 5.91$ (purple dashed curve).

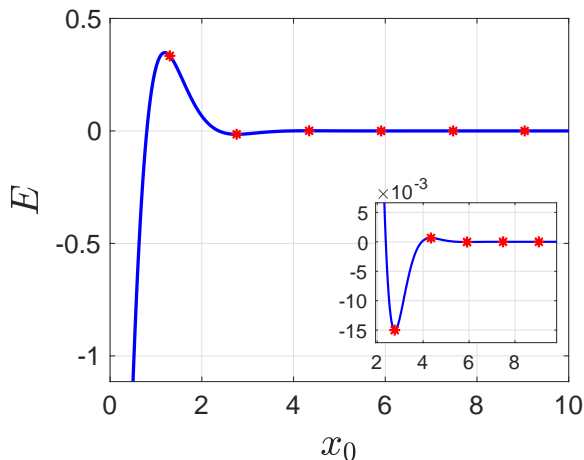


FIG. 3. Energy vs x_0 . Blue curve is $-2M(ae^{-2x_0}(\sin(2x_0 + b) + \cos(2x_0 + b)))/4$ with $M = 1.18519$, $a = 6.389$ and $b = 0.7549$, which is $2M \int A_K(x_0)dx_0$ where $A_K(x_0)$ is defined in Eq. (19). The red points are the normalized potential energies of the equilibria at $x_0=1.30, 2.76, 4.33, 5.91, 7.48, 9.04$, the first four of which are shown in Figure 2.

the $\dot{X}_{AK}(x_0)$ axis, which verifies the existence of the centers and saddles at the values given above. We also note the apparently self-similar nature of the phase portrait, exhibiting a qualitative repetition at progressively smaller scales, but do not pursue this further here.

For the PDE, Eq. (2), we expect that for $x_0 = 1.30$ and $x_0 = 4.34$, the equilibrium solutions shown in Figure 2 are locally unstable and those for $x_0 = 2.76$ and $x_0 = 5.91$ are locally stable. This is confirmed by Figure 5, where the spectral plots (λ_r, λ_i) are shown for the eigenvalues $\lambda = \lambda_r + i\lambda_i$ of the linearized field equation. Using the expansion $u(x, t) = u_0(x) + \epsilon e^{\lambda t} w(x)$ around an equilibrium solution $u_0(x)$ and solving for the eigenvalues λ and eigenvectors w , we conclude that the equilibrium is stable for $x_0 = 2.76$ and $x_0 = 5.91$, as all eigenvalues are imaginary, and that it is unstable for $x_0 = 1.30$ and $x_0 = 4.34$, as in that case there is one real eigenvalue pair. The lowest non-zero imaginary eigenvalue in the former case, as well as the single nonvanishing real pair in the latter case correspond to the mode associated with the relative motion of the kink and antikink centres, leading to stable oscillations in the former case and unstable sliding away in the latter. The vanishing pair of eigenvalues is associated with the rigid translation of

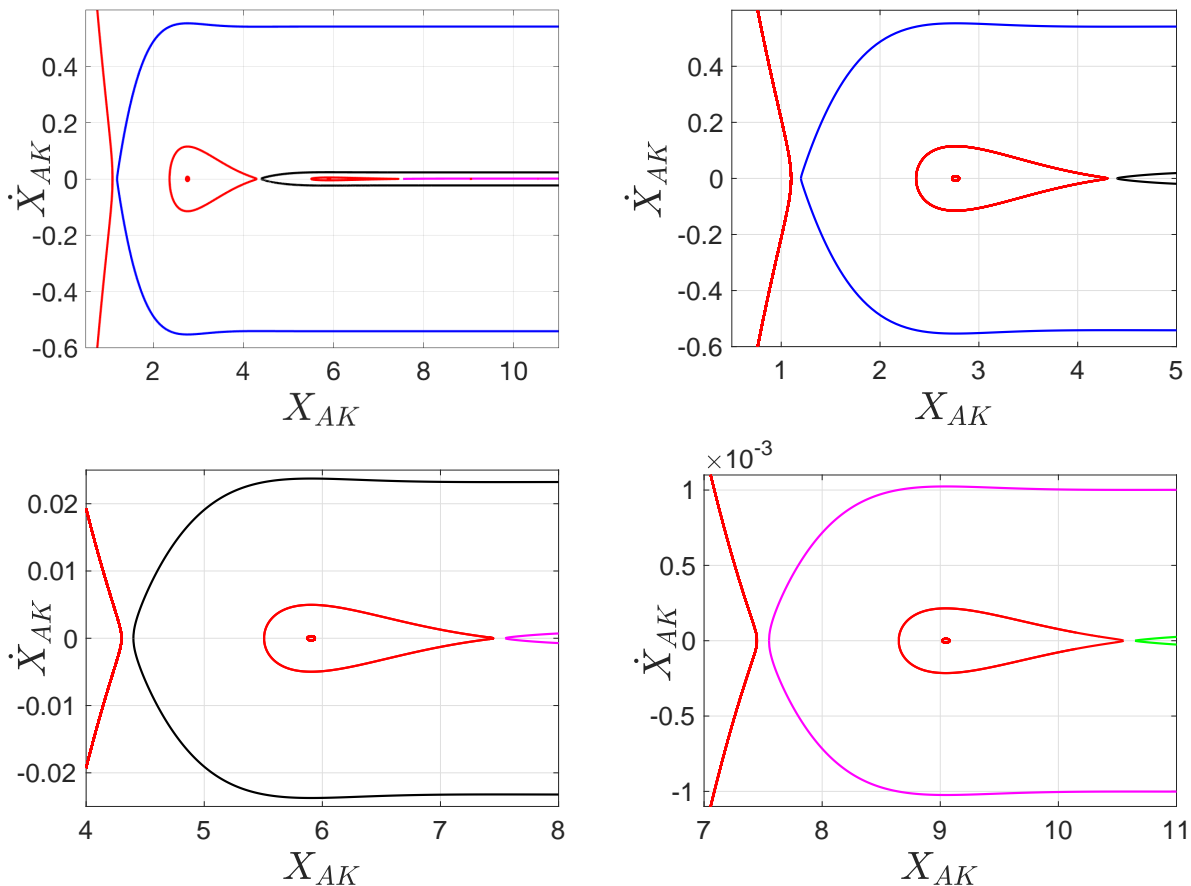


FIG. 4. Phase portrait of Equation (20) at different scales; colors in the top left panel correspond to colors in the other figures. Top left: Overall portrait for $0.5 \leq X_{AK}(x_0) \leq 11$ and $-0.6 \leq \dot{X}_{AK}(x_0) \leq 0.6$. Top right: Zoom to $0.5 \leq X_{AK}(x_0) \leq 5$ and $-0.6 \leq \dot{X}_{AK}(x_0) \leq 0.6$. Bottom left: Zoom to $4 \leq X_{AK}(x_0) \leq 8$ and $-0.025 \leq \dot{X}_{AK}(x_0) \leq 0.025$. Bottom right: Zoom to $7 \leq X_{AK}(x_0) \leq 11$ and $-0.0011 \leq \dot{X}_{AK}(x_0) \leq 0.0011$.

the kink-antikink pair, which is energy-neutral and whose eigenvector $w = u_x$ is the translation zero mode. Lastly, we note the presence of another nontrivial imaginary eigenvalue below the phonon band of spatially extended modes which appears to be analogous to the well-known internal excitation mode of the ϕ^4 Klein-Gordon kink [7–9].

B. Kink-Antikink Interactions with Non-Zero Initial Velocities

In [15] a kink and antikink were sent towards each other at various initial velocities v_{in} and the outgoing velocity v_{out} was recorded. For v_{in} up to a critical value of approximately 0.5108 it was found that the solitons rebound elastically ($v_{out} = v_{in}$), and for velocities greater than a second critical value of approximately 0.5896 the solitons interact once and then separate with $v_{out} < v_{in}$. Between these two critical values, the solitons get trapped and form a bion state. Furthermore, the kink and antikink appeared to approach and oscillate about a steady state when v_{in} was very close to the first or second critical value. We can now use the results of the present paper to explain some of these observations.

Using Eq. (20) of Section III A we can make some predictions about how the kink and antikink will interact, provided their separation does not get close to zero. From Figure 4 we predict that for $x_0 = 10$, the behaviour depends on the initial velocity. The initial velocity that creates the blue trajectory is about $v_{in} = -0.54$ as can be seen in the first two panels. Similarly, the initial velocities that create the black (magenta) trajectories are about $v_{in} = -0.023$ (-0.001) as can be seen from the third (final) panels. Thus in all cases, when $0.001 < |v_{in}| < 0.54$ we expect that the kink and antikink will approach each other up to a certain point, then reverse direction under the

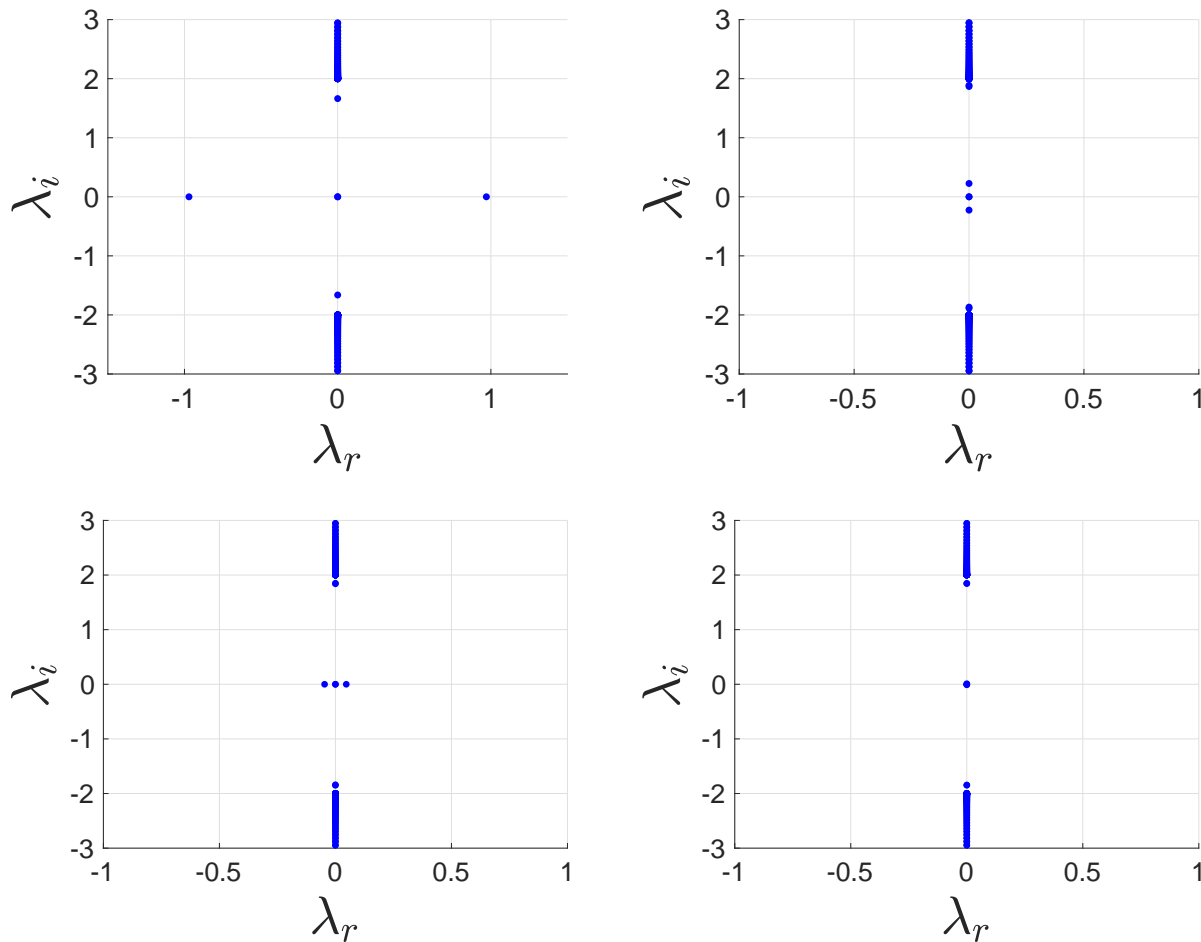


FIG. 5. The spectral plane (λ_r, λ_i) of eigenvalues $\lambda = \lambda_r + i\lambda_i$ of oscillations around the equilibria at $x_0 = 1.30$ (top left), $x_0 = 2.76$ (top right), $x_0 = 4.34$ (bottom left), $x_0 = 5.91$ (bottom right).

influence of one of the saddle points, eventually attaining the velocity $v_{\text{out}} = |v_{\text{in}}|$, so there is no loss of energy. The minimum kink-antikink separation depends on which saddle “turns back” the trajectory. Also, there will be a jump in the minimum separation near each of the v_{in} values given above.

For $x_0 = 10$ there is a further possibility. If $|v_{\text{in}}| < 0.001$, the trajectory will orbit the center at $x = 9.04$. Thus in the PDE simulation, we should see the kink and antikink both oscillating for all time. In this case there is no v_{out} . Oscillations can occur around any center with a smaller x_0 value, but this requires the kink and antikink to start closer together.

We turn now to the PDE simulations to see if our predictions based on the simple ODE model Eq. (20) hold. Figure (6) shows contour plots of the PDE, corresponding to three v_{in} values for a separation half-distance of $x_0 = 10$, and one v_{in} value with $x_0 = 3$. For each case, we also plot the solution to Eq. (20) in blue on top of the contour plot. In all cases, the simple model correctly predicts the motion of the center of the antikink in the PDE simulation. Note that in moving from the upper left panel, to the upper right panel, to the lower left panel of Figure 6 we see that the minimum approach distance transitions from about $x = 2$ to about $x = 5$; this corresponds to a transition from a phase-plot trajectory which is inside the blue trajectory in Figure 4 to a trajectory inside the black trajectory in that figure, bypassing the saddle at $x = 4.33$. Further reductions in the value of $|v_{\text{in}}|$ would show this process repeating, with the phase-plot trajectory bypassing the saddle at $x = 7.48$ (now inside the magenta trajectory) resulting in a minimum approach distance between approximately 7.48 and 8.5. If $|v_{\text{in}}|$ is reduced even further, the result is a trajectory around the center at $x = 9.04$. (The time for the PDE simulation to show oscillations about the center at $x = 2.76$ is rather large.) The bottom right panel shows a trajectory that encloses a different center, the one at $x = 2.76$.

The left boundary of the interval where multiple bounces occur, $|v_{\text{in}}| = 0.5109$, corresponds to the v_{in} value that

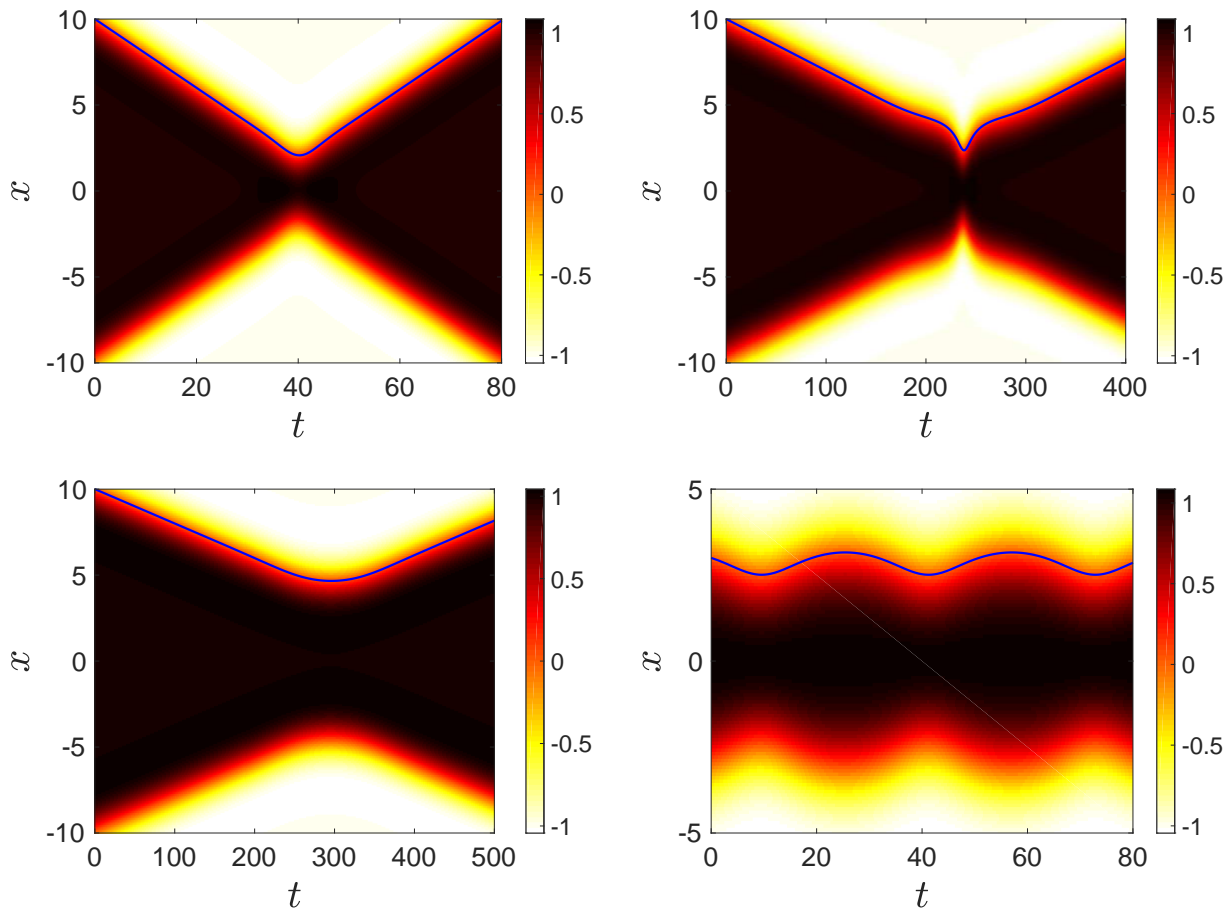


FIG. 6. Comparisons of the PDE contour plot of the displacement field $u(x, t)$ and the ODE trajectory solving Eq. 20 (blue solid curve). Upper left: $x_0 = 10$, $|v_{\text{in}}| = 0.2$. Upper right: $x_0 = 10$, $|v_{\text{in}}| = 0.03$. Lower left: $x_0 = 10$, $v_{\text{in}} = 0.02$. Lower right: $x_0 = 3$, $|v_{\text{in}}| = 0.05$.

creates the trajectory that approaches the saddle at $x = 1.3$. Note that this is somewhat inconsistent with the phase portraits in Figure 4 (top level) which indicates a value of about $v_{\text{in}} = -0.54$ (vertical coordinate of the blue trajectory at $x_0 = 10$). As noted previously, this is due to the fact that the saddle in the model given by Eq. (20) is at $x = 1.19$ but the unstable equilibrium in the PDE model is at $x_0 = 1.3$ (recall that for $x < 1.8$ the ODE model loses accuracy). Nevertheless, the asymptotic analytical formulation of Eq. (17) and the corresponding numerical finding of Eq. (19) provide a particularly useful energy landscape for kink-antikink collisions in our beam model.

IV. CONCLUSIONS AND FUTURE CHALLENGES

In the present work, we have examined the kink-antikink interaction in a nonlinear beam model with a ϕ^4 potential, i.e., a cubic nonlinearity. We have deployed an asymptotic methodology based on [6] to find the force acting between a kink and antikink, and hence their accelerations. The oscillatory tails of these structures (as discovered in [15]) imply that there is an exponentially modulated, spatially oscillatory force alternating between regions of attraction and repulsion. The saddles and centers of the effective dynamics with one degree of freedom, which are stationary points of an effective potential, are confirmed through PDE computations. The predicted kink and antikink accelerations are also confirmed by direct numerical computations using the PDE. In addition, the collision dynamics implied by the kink-antikink potential energy landscape is found to be in good agreement with direct PDE time evolution simulations, except when the separation is very small.

There are numerous directions in which one could extend this work. We did not yet study the interplay of the translational motion of the kink and antikink with the internal mode that kinks in this nonlinear beam model appear

to possess, according to our stability analysis. It would also be interesting to relate our work to recent studies of experimentally relevant pure-quartic solitons, and of the effect of mixed second and fourth derivatives in the NLS realm [20, 21]. Lastly, it would be interesting to seek models in higher dimensions where other types of solitary waves, for example, vortices, have a potential energy landscape with multiple stationary points.

ACKNOWLEDGEMENTS

NSM is partially supported by STFC consolidated grant ST/P000681/1. This material is based upon work supported by the US National Science Foundation under Grants No. PHY-1602994 and DMS-1809074 (PGK). PGK also acknowledges support from the Leverhulme Trust via a Visiting Fellowship and thanks the Mathematical Institute of the University of Oxford for its hospitality during part of this work.

-
- [1] T.I. Belova and A.E. Kudryavtsev, Solitons and their interactions in classical field theory, *Phys. Usp.*, **40**, 359 (1997).
 - [2] D.K. Campbell, Historical overview of the ϕ^4 model, in P.G. Kevrekidis and J. Cuevas-Maraver (Eds.), *A dynamical perspective on the ϕ^4 Model*, Springer-Nature (Heidelberg, 2019).
 - [3] P.G. Kevrekidis and R.H. Goodman, Four Decades of Kink Interactions in Nonlinear Klein-Gordon Models: A Crucial Typo, Recent Developments and the Challenges Ahead, <https://dsweb.siam.org/The-Magazine/All-Issues/acet/1/archive/10-2019> (2019).
 - [4] I. Takiy and H. Weigel, Collective coordinates in one-dimensional soliton models revisited, *Phys. Rev. D*, **94**, 085008 (2016).
 - [5] C.F.S. Pereira, G. Luchini, T. Tassis, and C.P. Constantinidis, Some novel considerations about the collective coordinates approximation for the scattering of ϕ^4 kinks, arXiv:2004.00571.
 - [6] N.S. Manton, An effective Lagrangian for solitons, *Nucl. Phys. B*, **150**, 397 (1979).
 - [7] T. Sugiyama, Kink-antikink collisions in the two-dimensional ϕ^4 model, *Prog. Theor. Phys.*, **61**, 1550 (1979).
 - [8] D.K. Campbell, J.S. Schonfeld, and C.A. Wingate, Resonance structure in kink-antikink interactions in ϕ^4 theory, *Physica D*, **9**, 1 (1983).
 - [9] P. Anninos, S. Oliveira, and R.A. Matzner, Fractal structure in the scalar $\lambda(\phi^2 - 1)^2$ theory, *Phys. Rev. D*, **44**, 1147 (1991).
 - [10] R.H. Goodman and R. Haberman, Kink-antikink collisions in the ϕ^4 equation: The n -bounce resonance and the separatrix map, *SIAM J. Appl. Dyn. Sys.*, **4**, 1105 (2005).
 - [11] R.H. Goodman, Chaotic scattering in solitary wave interactions: A singular iterated-map description, *Chaos*, **18**, 023113 (2008).
 - [12] H. Weigel, Kink-antikink scattering in ϕ^4 and ϕ^6 models, *J. Phys. Conf. Ser.*, **482**, 012045 (2014).
 - [13] P.G. Kevrekidis and J. Cuevas-Maraver (Eds.), *A Dynamical Perspective on the ϕ^4 model*, Springer Nature (Heidelberg, 2019).
 - [14] A. Demirkaya and M. Stanislavova, Numerical results on existence and stability of standing and traveling waves for the fourth order beam equation, *Discrete Contin. Dyn. Syst. B*, **24**, 197 (2019).
 - [15] R. Decker, A. Demirkaya, P.G. Kevrekidis, D. Iglesias, J. Severino, and Y. Shavit, Kink dynamics in a nonlinear beam model, arXiv:2001.06973.
 - [16] S. Levandosky, Stability and instability of fourth order solitary waves, *J. Dynam. Diff. Eqs.*, **10**, 151 (1998).
 - [17] A.R. Champneys, P.J. McKenna, and P.A. Zegeling, Solitary waves in nonlinear beam equations: stability, fission and fusion, *Nonlinear Dynamics*, **21**, 31 (2000).
 - [18] Y. Chen and P.J. McKenna, Traveling waves in a nonlinearly suspended beam: theoretical results and numerical observations, *J. Diff. Eqs.*, **136**, 325 (1997).
 - [19] P. Karageorgis and P.J. McKenna, The existence of ground states for fourth-order wave equations, *Nonlinear Anal.*, **73**, 367 (2010).
 - [20] A. Blanco-Redondo, C. Martijn de Sterke, J.E. Sipe, T.F. Krauss, B.J. Eggleton, and C. Husko, Pure-quartic solitons, *Nature Comms.*, **7**, 10427 (2016).
 - [21] K.K.K. Tam, T.J. Alexander, A. Blanco-Redondo, and C.M. de Sterke, Generalized dispersion Kerr solitons, *Phys. Rev. A*, **101**, 043822 (2020).
 - [22] X. Gràcia and T. Sanz-Perela, The wave equation for stiff strings and piano tuning, *Reports@SCM* **3**, 1 (2017).
 - [23] I. Posukhovskiy and A. Stefanov, On the normalized ground states for the Kawahara equation and a fourth order NLS, arXiv:1711.00367.
 - [24] N. Manton and P. Sutcliffe, *Topological Solitons*, Cambridge University Press (Cambridge, 2004).
 - [25] L.N. Trefethen, *Spectral Methods in MATLAB*, SIAM (Philadelphia, 2000).
 - [26] I.C. Christov, R. Decker, A. Demirkaya, P.G. Kevrekidis, and V.A. Gani, Long range interactions of kinks, *Phys. Rev. D*, **99**, 016010, (2019).